Aggregation and Coarsening of Ligand-Stabilized Gold Nanoparticles in Poly(methyl methacrylate) Thin Films

Luciana Meli[†,‡] and Peter F. Green[‡,*]

[†]Department of Chemical Engineering, The University of Texas at Austin, Austin, Texas 78712, and [‡]Department of Materials Science and Engineering, The University of Michigan, Ann Arbor, Michigan 48109

ABSTRACT Dodecanethiol-stabilized gold nanoparticles (5 nm diameter) are shown to self-organize to form a two-dimensional hexagonal structure in poly(methyl methacrylate) films upon spin-casting from solution onto a substrate, using high-angle annular dark-field scanning transmission electron microscopy. Through use of the distribution functions describing particle distributions, we show that the particle coarsening dynamics is self-similar, characterized by two distinct growth stages. During the initial stage, coarsening occurs *via* simultaneous Ostwald ripening and coalescence mechanisms, whereas during the second stage, the dominant coarsening mechanism is coalescence.

KEYWORDS: polymer nanocomposite · coarsening mechanisms · Ostwald ripening · coalescence · nanoparticle · thin film · dodecanethiol desorption

The fabrication of polymer-based nanocomposites through the incorporation of inorganic particles throughout a polymer host is now a widespread strategy to improve the performance of polymer systems in a vast range of applications. Significant property enhancements,[1–9] viscosity, diffusion, glass transition, wetting, interfacial processes, optical, thermal, electrical, and mechanical properties are exhibited by these nanocomposites, particularly when the dimensions of the particles are comparable to the average chain dimension of the polymer, R_g.[8,10–13] In this paper we examine, for the first time, the structural evolution (coarsening) of the size of dodecanethiol-functionalized gold nanocrystals embedded in a thin film of a polymer, poly(methyl methacrylate) (PMMA).

Coarsening is a ubiquitous phenomenon, responsible for a diverse range of processes that include aerosol aggregation,[14,15] phase separation of liquid−liquid mixtures,[16,17] and the morphology of thin metallic and semiconductor films on substrates.[18–21] Two general mechanisms have been proposed to explain late-stage coarsening behavior: Ostwald ripening (OR) and coalescence. In the classic OR growth mechanism, particles grow through the transfer of atoms/molecules from smaller particles to larger particles. Transport is due to differences between the chemical potentials, μ, of the particles; μ varies as the particle radius of curvature. Dynamic coalescence, on the other hand, involves the collective motion of particles or clusters that grow upon collision; the mean cluster size increases with time. The growth process is self-similar for both mechanisms, and the average radius, R, of the particles in the system may be characterized by a single length scale: $\langle R \rangle \propto t^{\beta}$, where the value of the exponent can provide insight into the mechanism of the growth process.

We show that nanoparticles which initially self-assembled from solution to form a two-dimensional hexagonal close-packed structure in a thin polymer film coarsened upon annealing at elevated temperatures. The structural evolution was characterized by two stages: an initial stage wherein growth is due to simultaneous mechanisms, OR and coalescence, and a later growth stage characterized by a scale-invariant distribution reminiscent of growth by coalescence alone. The transition between the growth stages is evidently facilitated by desorption of the dodecanethiol ligands. To the best of our knowledge, this is the first study of nanoparticle coarsening in a polymer system showing that the growth process is well-described by classical coarsening mechanisms.

RESULTS

A scanning transmission electron microscopy (STEM), *Z*-contrast image of the as-cast PMMA/Au nanocomposite film is presented in Figure 1a, where it is evident that the gold nanoparticles initially form self-

*Address correspondence to pfgreen@umich.edu.

Received for review January 23, 2008 and accepted May 21, 2008.

Published online June 5, 2008.
10.1021/nn800045s CCC: $40.75

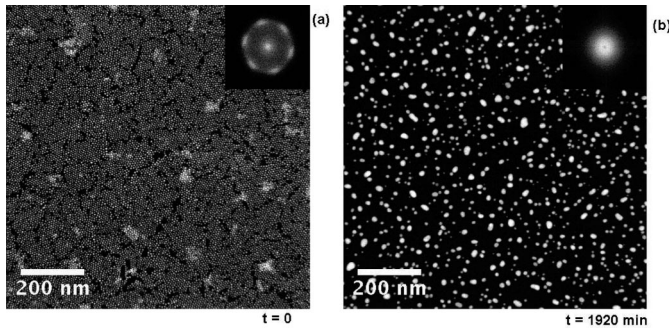

Figure 1. High-angle annular dark-field images illustrating the morphologies of PMMA/gold nanoparticle nanocomposite films. (a) The as-cast film presents a self-assembled two-dimensional network of Au nanocrystals, with some nanoparticle bilayer domains (brighter regions). The 2D Fourier power spectrum included as an inset confirms hexagonal symmetry in the lattice. (b) The image depicts coarsening of the gold nanoparticles after annealing the film in vacuum environments at $T = 150$ °C. The power spectrum demonstrates loss of order in the nanoparticle array.

organized, two-dimensional hexagonal structure. The 2D Fourier transform power spectrum included as an inset confirms that the packing exhibits hexagonal symmetry. The average edge-to-edge distance is 1.9 nm, revealing interdigitation of the alkyl chains, given that the length of a dodecane chain is calculated to be 1.77 nm.[22]

Dynamic secondary ion mass spectrometry (DSIMS) measurements of a nanocomposite film reveal that the gold nanocrystals are segregated at the free surfaces. Further evidence of this interfacial segregation is observed in scanning force microscopy (SFM) images of the as-cast film, which possess a relatively large root-mean-square roughness (1.9 nm) with features of depth comparable to the size of the nanoparticles (see Supporting Information). The colloidal nanocrystals are segregated exclusively at the free surface due to the relatively low surface tension of the dodecanethiol ligands ($\gamma_{DT} = 25.4$ mJ/m^2) with respect to that of PMMA ($\gamma_{PMMA} = 40.2$ mJ/m^2). This is better understood by considering that the adsorption energy of a particle at an interface[23,24] is given by $E_a = \pi R_{eff}^2 \gamma_{PMMA}(1 - |\cos\theta|)^2$, where $\cos\theta = (\gamma_{DT} - \gamma_{DT\text{-}PMMA})/\gamma_{PMMA}$, and R_{eff} is the radius of the coated particle (gold core radius plus brush thickness). The particle/interface interaction is strongest when $\cos\theta = 1$. Here, $\gamma_{DT\text{-}PMMA} = 5.2$ mJ/m^2 and $R_{eff} \approx 4.1$ nm, which reveals that $E_a \gg 10kT$. Clearly, the energy required to remove a particle from the free surface of the film is large compared to the thermal energy; hence, the particles are expected to be bound at this interface. When these particles segregate to the free surface of a film, they typically exhibit hexagonal packing. To this end, the hexagonal pattern formation is consistently observed at sufficiently high packing densities in solution-cast polymer thin film systems that include other polymers such as polystyrene (PS) and polyvinylpyridine (PVP).

It is noteworthy that the dynamics of the organization of nanoparticles has been studied by a number of authors;[25–27] specifically, the controlled drying of particle solution mixtures on solid substrates was examined. However, to our knowledge, the formation of self-assembled monolayers (SAMs) of nanoparticles on polymer surfaces, through rapid evaporation (spin-coating) of polymer/nanoparticle solutions, has never been demonstrated and therefore requires further study. Ultimately, a clear understanding of the dynamics of nanoparticle formation on the polymer matrix would be desirable to produce transferable self-assembled nanocrystalline monolayers with improved long-range order.

After annealing the nanocomposite film in a vacuum at 150 °C for a period of 1920 min, it is evident, even from the low-magnification image presented in Figure 1b, that the particles have coarsened considerably and that the hexagonal order which the particle array initially exhibited no longer exists (see Figure 1b inset). Higher-magnification high-angle annular dark-field (HAADF) images of the nanocomposite film, along with a plot of the probability distribution of particle sizes at two different times (Figure 2), show more clearly the increase of particle size with annealing time. It is also clear that particles become more irregular at long times ($t = 5700$ min), as observed when examining the plot of the average shape factor, S_f, *versus* time (Figure 3), which provides a measure of the relative circularity of planar shapes ($S_f = 1$ for a circle).

To gain insight into the mechanism of coarsening of the gold nanoparticles in the films, we examined the time dependencies of the average particle radius, $\langle R(t)\rangle$, and the number of particles, $N(t)$. Both quantities seem to exhibit a power-law dependence on time, showing that the growth of gold cores with annealing time, as described by $\langle R(t)\rangle$, is naturally accompanied by a decrease in the $N(t)$. The value of the power-law exponent for the former is 0.192, while that for the latter is -0.627 (see Supporting Information). Conservation of mass defines the relationship between $N(t)$ and $\langle R(t)\rangle$. Assuming that the characteristic length R scales as $m^{1/D}$, where m is the mass of the aggregate and D is its fractal dimension (equal to 3 for the compact, approximately spherical clusters obtained after shape relaxation), then $\langle R(t)\rangle^3 N(t)$ is approximately constant, as confirmed from their time dependence. Thus, the coarsening exponent, β, is given by $\langle R(t)\rangle \propto t^{\beta}$ and $N(t) \propto t^{-3\beta}$. Based on the mean-field theory of OR, $\beta = {}^1/_2$ in dimensionally homogeneous systems (2D/2D and 3D/3D systems) when the rate limiting step for transport is associated with detachment of atoms, while $\beta = {}^1/_3$ when transport is limited by surface diffusion of the species.[28,29] For 3D particles in a 2D diffusion field, a divergence in the steady-state solution of the 2D diffusion equation complicates the analysis.[30] However, an asymptotic growth exponent $\beta = {}^1/_4$ has been found when transport is determined by dif-

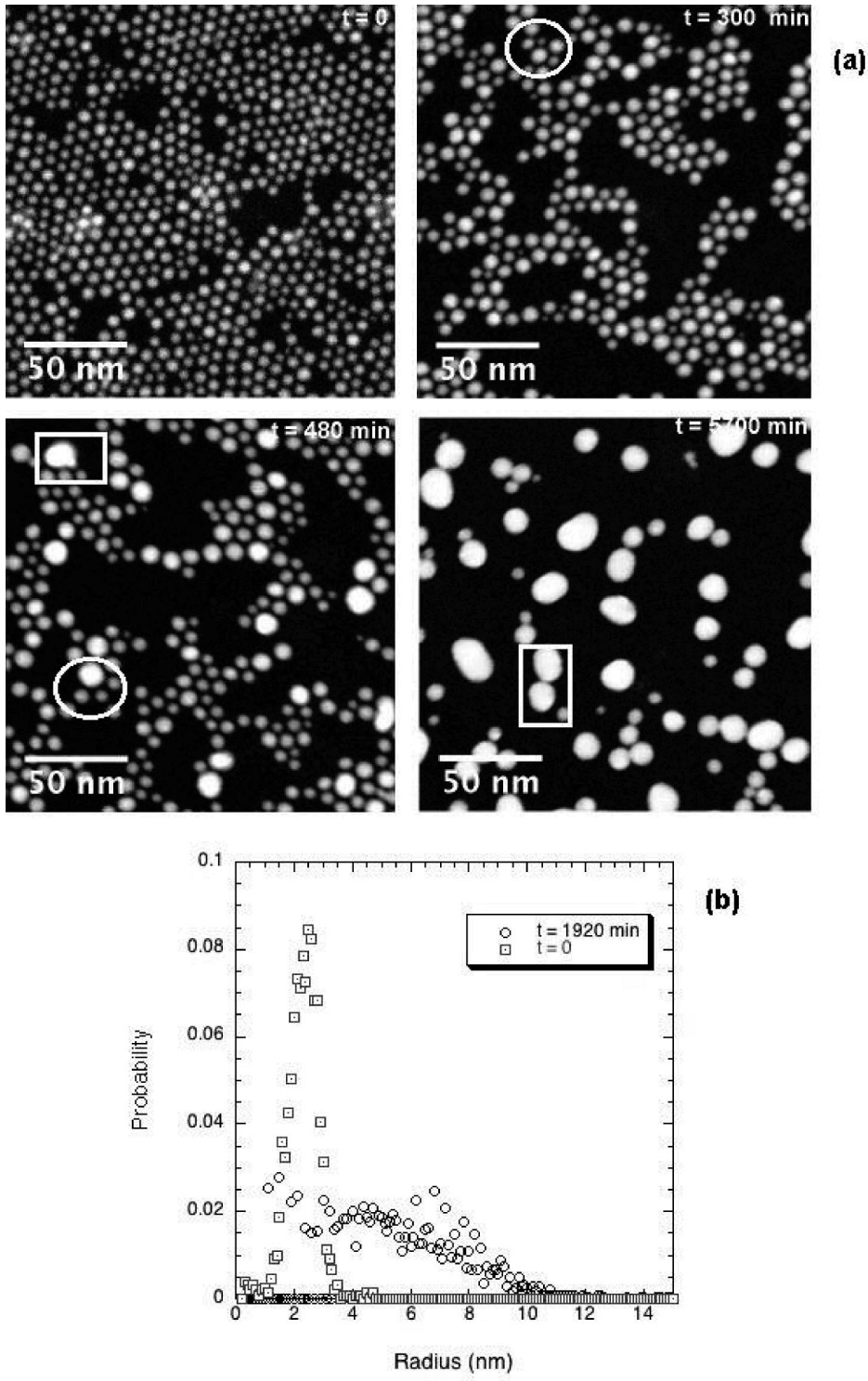

Figure 2. (a) Evolution of particle size within the film processed in vacuum environments (T = 150 °C), shown in the HAADF images at four different annealing times. (b) Coarsening of the nanoparticles captured in the broadening of (non-normalized) distribution of nanoparticle sizes with time.

fusion. On the other hand, for interface-limited mass transport in 3D/2D systems, it was found that $\beta = {}^1/_3$.[18] Thus, the experimental value of the coarsening exponent revealed by our experiments, $\beta \approx {}^1/_5$, suggests that the coarsening process is not exclusively driven by capillarity.

DISCUSSION

It is well known that the value of the power-law exponent is sometimes insufficient to deduce the mechanism that engenders coarsening.[31] However, theory shows that each mechanism leads to distinct scale-invariant distribution functions for the particle size, $F(R/$

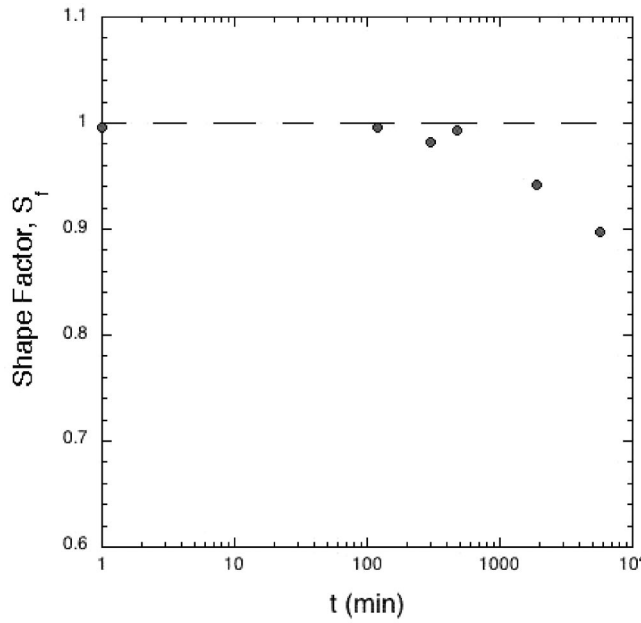

Figure 3. Time dependence of the shape factor, S_f.

$\langle R \rangle$) *vs* $R/\langle R \rangle$, in the asymptotic limit ($t \rightarrow \infty$). Accordingly, we now analyze the nanoparticle size distribution function of the vacuum-annealed nanocomposite film by normalizing the cluster size frequency distribution at each time (Figure 4). It is noteworthy that all the data did not collapse onto a single curve, as expected for a self-similar coarsening process. The normalized distribution functions that characterize the structure at earlier times, $t \approx 120-480$ min, are relatively narrow and symmetric. The probability distributions at later times ($t = 1920$ and 5700 min) collapsed perfectly onto a single curve, exhibiting a log-normal shape that is positively skewed. Moreover, the non-logarithmic plot of $\langle R \rangle$ *vs* t (Figure 5a) shows that the coarsening kinetics of the particles can be divided into two distinct growth stages, with a discontinuity at ~480 min. In the following, we will examine both regimes separately.

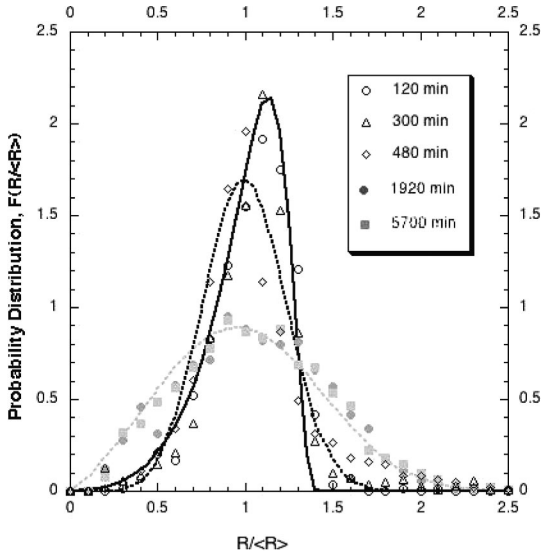

Figure 4. Comparison of the theoretical and experimental normalized distribution functions. The experimental distributions at five different annealing times are plotted with unfilled markers for the early growth stage, and with filled gray markers for late-stage growth ($t > 480$ min). The solid black line represents the distribution characteristic of diffusion-limited OR, and the dotted lines are the Smoluchowski distributions that best fit the data at each of the stages: the black curve corresponds to $t < 480$ min, with $\alpha = -1.6$, and the gray curve corresponds to $t > 480$ min, with $\alpha = -0.1$.

The experimental particle distribution at earlier times show the best agreement with the diffusion-controlled OR equation:

$$F(R' = R/\langle R \rangle) = \begin{cases} \dfrac{4R'^2}{9}\left(\dfrac{3}{3+R'}\right)^{7/3}\left(\dfrac{-3/2}{R'-3/2}\right)^{11/3}\exp\left(\dfrac{R'}{R'-3/2}\right) & \text{if } R' < 3/2 \\ 0 & \text{if } R' > 3/2 \end{cases} \quad (1)$$

For example, at time $t = 120$ min, the calculated R-squared error between the experimental distribution and eq 1 is $R^2 = 0.96$ (Figure 4). However, some features of the experimental curve, such as the slight tail extending to larger cluster sizes, are better captured by the analytical solution to the Smoluchowski equation, eq 2 ($R^2 = 0.91$, $\alpha = -1.6$):

$$F(R') = \frac{3W(R'W)^{-3\alpha+1}\exp[-(WR')^3]}{\Gamma(-\alpha+2/3)} \quad (2)$$

where $W = \Gamma(-\alpha + 1)/\Gamma(-\alpha + 2/3)$, and α is a scaling exponent that quantifies the dependence of the cluster diffusion coefficient with its mass. It is important to note that this long-time analytical solution is consistent with the expected power-law scaling behavior of the average particle size, $\langle R \rangle \sim t^{\beta}$, with $\beta = 1/(2 - 3\alpha)$.

We suggest that the distributions at earlier times are the result of simultaneous coalescence and ripening-based growth. The relative contributions of coalescence and condensation can be obtained from the moments of the nanocrystal size distribution, $\mu_1 = R_3/R_h$ and $\mu_3 = \langle R \rangle/R_3$, where $\langle R \rangle$ is the arithmetic mean radius, $\langle R \rangle = \sum R_i/n$, R_3 is the cube-mean radius, $R_3 = (\sum R_i^3/n)^{1/3}$, and R_h is the harmonic mean radius, $R_h = n/\sum(1/R_i)$.[32] Both moments are unity for monodisperse particles obtained by condensation, while for $\mu_1 > 1.25$ and $\mu_3 < 0.905$ growth occurs only through coalescence.[32] If $1 < \mu_1 < 1.25$ and $1 > \mu_3 > 0.905$, coarsening is achieved by a combination of both mechanisms. For the sample at $t = 120$ min, the moments of the particle size distribution were $\mu_1 = 1.117$ and $\mu_3 = 0.955$, indicating that both condensation and coalescence may play a role in the growth of the particles at this stage (Figure 5b).

It is worth mentioning that predictions of the mean-field model for ripening represented by eq 1 are valid for vanishingly small volume fractions. Simulations have shown that reductions in the height of the particle size

distribution characteristic of OR, as well as broadening of the profile, can be obtained at higher particle volume fractions.[33] Hence, the differences between our experimental data and the curve described by eq 1 could also be due to a non-negligible particle concentration. Despite this caveat, the agreement between experiment and theory is very good and provides the appropriate insight required for the dynamics of this system.

At much longer annealing times, the particle dimensions continue to increase in size (while the number of particles decreases) and the moments of the distribution gradually diverge from unity (Figure 5b) due to an increase in the polydispersity of the nanocrystals ($\sigma/\langle R\rangle_{t = 480\text{min}} \approx 30\%$). A close survey of the HAADF images of Figure 2a provides evidence of growth by OR in the initial stages. At $t = 300$ min, particles retain the very smooth, spherical shape typical of growth by ripening;[34] small particles ($R_i \ll \langle R\rangle$) reside close to large particles ($R_i \gg \langle R\rangle$), as exemplified by the circular region highlighted in the corresponding HAADF image. After an additional 3 h of annealing, at $t \approx 480$ min, the merging of particles in the image is clearly identifiable (square regions), in spite of the fact that most particles are not in contact with each other and retain their spherical shape (circular region). This suggests that, during this initial stage, growth occurs by simultaneous OR and coalescence, and that coalescence becomes more significant with annealing time. The latter statement is consistent with the increasing polydispersity of the particles with time, characteristic of coalescence-based growth.[35]

We now examine the mechanism of coarsening in the late stages of growth, for $t > 480$ min. The HAADF image corresponding to $t = 5700$ min in Figure 2a shows clusters characterized by irregular shapes (the value of S_f diverges from unity at $t > 480$ min, as seen in Figure 3), in direct contact with each other, revealing the predominance of coalescence events at later times. During this stage of growth, as mentioned earlier, the two normalized distribution functions collapse onto a single curve, manifesting the existence of a self-preserving distribution at long times. Not surprisingly, the line that fits our data best was calculated on the basis of the Smoluchowski solution with $\alpha = -0.1$ and $R^2 = 0.98$ (Figure 4). The small magnitude of the diffusion scaling exponent, α, indicates a weak dependence of the cluster diffusion coefficient with mass, but its negative value is still consistent with the notion that small particles should diffuse more rapidly than larger ones. From the asymptotic solution of the Smoluchowski equation given in eq 2, one also obtains the relation between α and β [$\beta = 1/(2 - 3\alpha)$], yielding a value of $\beta = 0.43$. This value should be equal to that obtained from the power-law exponent of $\langle R\rangle$ *vs* t at long times. Further experiments in this regime ($t > 480$ min) would be required to corroborate the consistency between the coarsening values obtained from the aforementioned plot and the fit to the particle size distribution. It should be noted that, at $t = 480$ min, the criteria $\mu_1 > 1.25$ and $\mu_3 < 0.905$ are met, supporting the theory that growth occurs exclusively through coalescence for $t > 480$ min (Figure 5b).

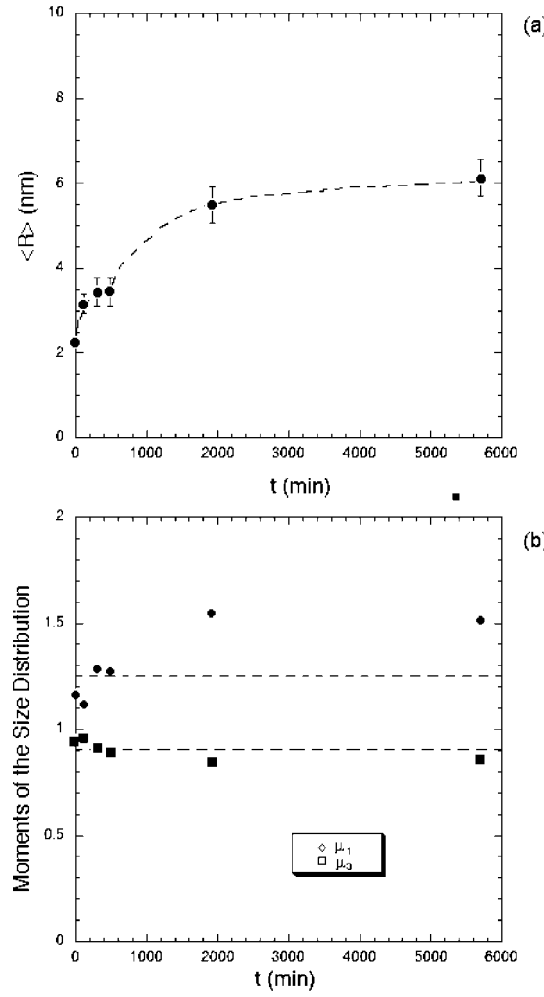

Figure 5. (a) Kinetics of nanoparticle growth due to thermal treatment ($T = 150$ °C), shown here in a linear plot of $\langle R\rangle$ *vs* t. The curve presents a discontinuity at ~500 min, suggesting the existence of two coarsening regimes. The dashed line is a guide to the eye. (b) First and third moments of the particle size distribution function, μ_1 (●) and μ_3 (), which gradually diverge from unity as the polydispersity of particles in the vacuum-annealed nanocomposite grows.

Thus far, we have not explained the reason for the two stages of kinetic growth described above. We suggest that the transition from simultaneous OR/coalescence-based growth to pure coalescence-based growth, at later times, is associated with the complete thermal desorption of the dodecanethiol ligands from the gold metal cores. At the beginning of the annealing process, particles are protected from aggregation and fusion by a layer of ligands that cover the gold core surface completely. As a general guideline, metallic cores are able to fuse if they approach to within a distance of 0.5 nm (δ_c) of each other.[36] From the HAADF images of the film at the earlier annealing times, the interparticle separation distance was measured to be $\delta = 1.9$

nm. Clearly, at this spacing the nanocrystals are not able to come into sufficient proximity to coalesce. On the other hand, atomic diffusion of gold atoms should be somewhat restricted by the presence of the dodecanthiol (DT) molecules, and growth through OR will also be inhibited.[37] During the course of the heating process, however, the ligands will gradually desorb (the desorption temperature of DT molecules from a Au(111) surface in a vacuum is ~120 °C)[37] and particles would only be partially passivated. Diffusion of free atoms, and small oligomers no longer bound by ligands, will promote growth by OR. As DT desorption continues, the partially passivated particles will have an increasing probability of coming within δ_c and fuse upon collision. Thus, OR and coalescence would occur simultaneously. At longer times at elevated temperatures, most ligands would have been thermally desorbed, and collisions would lead to coalescence; this mechanism would therefore dominate the growth of particles during this latter stage. We find evidence that total thermal desorption of ligands in our nanocomposite film occurred after 480 min, since in the HAADF image for this time there is clear evidence that particles are separated by a distance close to δ, the thickness of the steric barrier at time $t = 0$.

This is consistent with the results of studies of the structural transformation of Au(111) surfaces, with monolayer-high islands, covered by a SAM of DT molecules in a vacuum over a temperature range that includes room temperature and the desorption temperature.[37] These studies show that, at room temperature, atomic diffusion is completely inhibited by the thiol molecule, but as temperature increases to ~90 °C, the gold islands start growing through Ostwald ripening. Upon a further increase in temperature (~125 °C), rapid island growth was found to accompany the desorption of thiol molecules. Events of island−terrace fusion were often observed in the STM images, strongly suggesting the existence of growth by coalescence.

It should be noted that, in this system, the kinetics of desorption of the alkanethiol SAM from the gold surface are expected to be fast (on the order of minutes), considering the rapid structural transformation observed. However, in our system, the presence of the polymer matrix is responsible for slowing down the desorption rate of DT molecules. In fact, thermogravimetric analysis of a similar nanocomposite system composed of phenylethanethiol-coated gold nanoparticles in a PS-PVP matrix[38] indicated a weight loss of less than 50% of the total thiol ligands initially present upon annealing the sample at 170 °C for more than 8 h. Further insight into this issue would be gained by understanding the influence of the ligand surface coverage on the interaction energy between colloidal gold particles in a PMMA matrix, using the DLVO theory as the basis for studying the colloidal stability.[39] The form of the potential would ultimately give us information about the collision efficiency (the probability that particles adhere upon collision), as well as the reversibility of the aggregation process as a function of ligand coverage. A more complete theoretical picture of the problem at hand would require accounting for possible adsorption of polymer to the gold surface. This, or course, does not change the basic physics, coarsening *via* Ostwald Ripening and by coalescence, that characterizes the behavior of our system.

Some final considerations that may affect the analysis of the kinetics of growth of the nanoparticles in our system are related to the fact that some assumptions in our coarsening models may be violated in our system. First, the collisions between particles are not always binary, as assumed in the coalescence model. Most importantly, the coalescence model described above is strictly valid for particles that are randomly distributed in space, which is clearly not the case for our particles at the initial stages of growth. In the same manner, particle interactions and spatial correlations have also been shown to have an effect on the shape of the size distribution function in ripening-based growth, as mentioned before.[33] These are generally not first-order effects. Hence, the most remarkable finding is that the classical coarsening mechanisms provide a very good description of the size evolution of the particles in our system.

CONCLUSIONS

We presented the first experimental accounts of nanoparticle coarsening in thin polymer films in the nanometer thickness range. Analysis of the growth kinetics, the particle size distribution function, $F(R/\langle R\rangle)$ *vs* $R/\langle R\rangle$, and the spatial distribution and shape characteristics of the nanoparticles *via* HAADF images shows evidence of two distinct stages of growth; the transition between the stages is associated with a gradual desorption of the alkanethiol molecules at the high annealing temperature. We are currently studying nanoparticle coarsening processes in different environments. We hope that this study generates theoretical work on the structural evolution of nanoparticles in different environments.

METHODS

Gold nanocrystals stabilized with DT were synthesized by a modification of the two-phase arrested precipitation method reported by Brust *et al.*[40] using a 1/1 DT/$HAuCl_4$ ratio. The gold cores had an average diameter of 4.68 nm with a relatively broad size distribution, $\sigma/\langle R\rangle_{t=0} \approx 21\%$, as determined by HAADF imaging using STEM.

The gold particles were used to prepare composite solutions with poly(methyl methacrylate) (PMMA, Polymer Source, Inc., $M_w = 92\,000$ g/mol, $M_w/M_n = 1.08$) in toluene (Fisher Scien-

tific), yielding a concentration of polymer in solution of 2 wt %. The weight fraction of nanoparticles in the homopolymer was 13 wt %. Films with thicknesses of 200 nm were prepared by spin-coating the composite solution onto glass substrates of roughly 1 cm^2 at a spin rate of 1000 rpm. After spin-coating, the films were floated on water and off the glass substrate and then deposited onto transparent silicon nitride windows (SPI Supplies) with the use of a water lens held by a looped wire. Once prepared, the samples were annealed in a vacuum at 65 °C for a period of 30 h to remove excess solvent. Additional PMMA/Au nanocomposite films were spin-coated directly on silicon substrates with a silicon nitride layer of 100 nm grown by LPCVD (WaferNet, Inc.) for DSIMS analysis.

The films were then annealed above the glass transition temperature in a vacuum (100 mTorr) and subsequently quenched to room temperature. Following each annealing period, the samples were characterized with a combination of SFM and STEM. *Ex situ* images of the topography of the films were taken with Nanoscope IV scanning force microscope operating in tapping mode.

The spatial distribution and size of the gold nanoparticles within the homopolymer films were analyzed with a JEOL 2010F transmission electron microscope operating at an accelerating voltage of 200 kV in scanning mode (STEM) using a HAADF detector. Images for particle size measurement were acquired in at least three different regions of the sample. The images were then thresholded and treated with several digital filters using Clemex Vision image analysis software v2.2 (Clemex Technologies, Inc.) as well as Image J software. On average, 1400 particles were measured for determination of the particle size distribution at each annealing period. The average radius per particle $\langle R(t) \rangle$ (obtained from the projected, planar surface area of the particles, S, assuming $R(t) = (S(t)/\pi)^{1/2}$), the shape factor, S_f (defined such that $S_f = 4\pi S/P^2$, where P is the perimeter of the particle), and the number of particles per unit area, $N(t)$, were calculated at various stages during the coarsening of the particles.

Acknowledgment. Support from the U.S. Department of Energy (DOE #DE-FG02-07ER46412) is gratefully acknowledged. L.M. acknowledges support by the STC Program of the National Science Foundation under agreement CHE-9876674 and NSF DMR-0601890 for the first phase of this study involving nanoparticle synthesis and size characterization. She also acknowledges the assistance of Hyun Joon Oh at the University of Michigan.

Supporting Information Available: DSIMS depth profile of gold in an as-cast nanocomposite film, topography of the as-cast film from SFM in tapping mode, and plot of $\langle R(t) \rangle$ and $N(t)$ *vs* log t. These materials are available free of charge *via* the Internet at http://pubs.acs.org.

.

REFERENCES AND NOTES

1. Bliznyuk, V.; Ruhstaller, B.; Brock, P. J.; Scherf, U.; Carter, S. A. Self-Assembled Nanocomposite Polymer Light-Emitting Diodes with Improved Efficiency and Luminance. *Adv. Mater.* **1999**, *11*, 1257–1261.
2. Buxton, G. A.; Lee, J. Y.; Balazs, A. C. Computer Simulation of Morphologies and Optical Properties of Filled Diblock Copolymers. *Macromolecules* **2003**, *36*, 9631–9637.
3. Krishnamoorti, R.; Yurekli, K. Rheology of Polymer Layered Silicate Nanocomposites. *Curr. Opin. Colloid Interface Sci.* **2001**, *6*, 464–470.
4. Krishnan, R. S.; Mackay, M. E.; Hawker, C. J.; Van Horn, B. Influence of Molecular Architecture on the Dewetting of Thin Polystyrene Films. *Langmuir* **2005**, *21*, 5770–5776.
5. Li, C. X.; Wu, J. T.; Zhao, J.; Zhao, D. L.; Fan, Q. R. Effect of Inorganic Phase on Polymeric Relaxation Dynamics in Pmma/Silica Hybrids Studied by Dielectric Analysis. *Eur. Polym. J.* **2004**, *40*, 1807–1814.
6. Mackay, M. E.; Dao, T. T.; Tuteja, A.; Ho, D. L.; Van Horn, B.; Kim, H. C.; Hawker, C. J. Nanoscale Effects Leading to Non-Einstein-Like Decrease in Viscosity. *Nat. Mater.* **2003**, *2*, 762–766.
7. Papakonstantopoulos, G. J.; Yoshimoto, K.; Doxastakis, M.; Nealey, P. F.; de Pablo, J. J. Local Mechanical Properties of Polymeric Nanocomposites. *Phys. Rev. E* **2005**, *72*, 0318011−0318016.
8. Starr, F. W.; Schroder, T. B.; Glotzer, S. C. Effects of a Nanoscopic Filler on the Structure and Dynamics of a Simulated Polymer Melt and the Relationship to Ultrathin Films. *Phys. Rev. E* **2001**, *6402*, 0218021−0218025.
9. Sternstein, S. S.; Zhu, A. J. Reinforcement Mechanism of Nanofilled Polymer Melts as Elucidated by Nonlinear Viscoelastic Behavior. *Macromolecules* **2002**, *35*, 7262–7273.
10. Usuki, A.; Hasegawa, N.; Kato, M. Polymer-Clay Nanocomposites. *Adv. Polym. Sci.* **2005**, *179*, 135–195.
11. Coleman, J. N.; Khan, U.; Gun'ko, Y. K. Mechanical Reinforcement of Polymers Using Carbon Nanotubes. *Adv. Mater.* **2006**, *18*, 689–706.
12. Ganesan, V.; Pryamitsyn, V.; Surve, M.; Narayanan, B. Noncontinuum Effects in Nanoparticle Dynamics in Polymers. *J. Chem. Phys.* **2006**, *124*, 2211021–2211024.
13. Schmidt, G.; Malwitz, M. M. Properties of Polymer-Nanoparticle Composites. *Curr. Opin. Colloid Interface Sci.* **2003**, *8*, 103–108.
14. Mukherjee, D.; Sonwane, C. G.; Zachariah, M. R. Kinetic Monte Carlo Simulation of the Effect of Coalescence Energy Release on the Size and Shape Evolution of Nanoparticles Grown as an Aerosol. *J. Chem. Phys.* **2003**, *119*, 3391–3404.
15. Jeong, J. I.; Choi, M. A Bimodal Particle Dynamics Model Considering Coagulation, Coalescence and Surface Growth, and Its Application to the Growth of Titania Aggregates. *J. Colloid Interface Sci.* **2005**, *281*, 351–359.
16. Siggia, E. D. Late Stages of Spinodal Decomposition in Binary-Mixtures. *Phys. Rev. A* **1979**, *20*, 595–605.
17. Martula, D. S.; Hasegawa, T.; Lloyd, D. R.; Bonnecaze, R. T. Coalescence-Induced Coalescence of Inviscid Droplets in a Viscous Fluid. *J. Colloid Interface Sci.* **2000**, *232*, 241–253.
18. Zinke-Allmang, M. Phase Separation on Solid Surfaces: Nucleation, Coarsening and Coalescence Kinetics. *Thin Solid Films* **1999**, *346*, 1–68.
19. Semin, D. J.; Lo, A.; Roark, S. E.; Skodje, R. T.; Rowlen, K. L. Time-Dependent Morphology Changes in Thin Silver Films on Mica: A Scaling Analysis of Atomic Force Microscopy Results. *J. Chem. Phys.* **1996**, *105*, 5542–5551.
20. Floro, J. A.; Sinclair, M. B.; Chason, E.; Freund, L. B.; Twesten, R. D.; Hwang, R. Q.; Lucadamo, G. A. Novel Sige Island Coarsening Kinetics: Ostwald Ripening and Elastic Interactions. *Phys. Rev. Lett.* **2000**, *84*, 701–704.
21. Jeffrey, C. A.; Conrad, E. H.; Feng, R.; Hupalo, M.; Kim, C.; Ryan, P. J.; Miceli, P. F.; Tringides, M. C. Influence of Quantum Size Effects on Island Coarsening. *Phys. Rev. Lett.* **2006**, *96*, 1061051–1061054.
22. Pileni, M. P. Nanocrystal Self-Assemblies: Fabrication and Collective Properties. *J. Phys. Chem. B* **2001**, *105*, 3358–3371.
23. Chiu, J. J.; Kim, B. J.; Kramer, E. J.; Pine, D. J. Control of Nanoparticle Location in Block Copolymers. *J. Am. Chem. Soc.* **2005**, *127*, 5036–5037.
24. Dickson, J. L.; Binks, B. P.; Johnston, K. P. Stabilization of Carbon Dioxide-in-Water Emulsions with Silica Nanoparticles. *Langmuir* **2004**, *20*, 7976–7983.
25. Bigioni, T. P.; Lin, X. M.; Nguyen, T. T.; Corwin, E. I.; Witten, T. A.; Jaeger, H. M. Kinetically Driven Self Assembly of Highly Ordered Nanoparticle Monolayers. *Nat. Mater.* **2006**, *5*, 265–270.
26. Tang, J.; Ge, G. L.; Brus, L. E. Gas-Liquid-Solid Phase Transition Model for Two-Dimensional Nanocrystal Self-Assembly on Graphite. *J. Phys. Chem. B* **2002**, *106*, 5653–5658.
27. Lin, X. M.; Jaeger, H. M.; Sorensen, C. M.; Klabunde, K. J. Formation of Long-Range-Ordered Nanocrystal Superlattices on Silicon Nitride Substrates. *J. Phys. Chem. B* **2001**, *105*, 3353–3357.

28. Ardell, A. J. Temporal Behavior of the Number Density of Particles During Ostwald Ripening. *Mater. Sci. Eng. A-Struct.* **1997**, *238*, 108–120.
29. Carlow, G. R. Ostwald Ripening on Surfaces When Mass Conservation Is Violated: Spatial Cluster Patterns. *Physica A* **1997**, *239*, 65–77.
30. Shorlin, K.; Krylov, S.; Zinke-Allmang, M. Fundamental Problems Concerning Three Dimensional Clustering on Surfaces. *Physica A* **1998**, *261*, 248–265.
31. Lo, A.; Skodje, R. T. Kinetic and Monte Carlo Models of Thin Film Coarsening: Cross over from Diffusion-Coalescence to Ostwald Growth Modes. *J. Chem. Phys.* **2000**, *112*, 1966–1974.
32. Pich, J.; Friedlander, S. K.; Lai, F. S. The Self-Preserving Particle Size Distribution for Coagulation by Brownian Motion—III. Smoluchowski Coagulation and Simultaneous Maxwellian Condensation. *J. Aerosol Sci.* **1970**, *1*, 115–126.
33. Wang, K. G.; Glicksman, M. E.; Rajan, K. Length Scales in Phase Coarsening: Theory, Simulation, and Experiment. *Comput. Mater. Sci.* **2005**, *34*, 235–253.
34. Huang, F.; Zhang, H. Z.; Banfield, J. F. The Role of Oriented Attachment Crystal Growth in Hydrothermal Coarsening of Nanocrystalline ZnS. *J. Phys. Chem. B* **2003**, *107*, 10470–10475.
35. Madras, G.; McCoy, B. J. Distribution Kinetics of Ostwald Ripening at Large Volume Fraction and with Coalescence. *J. Colloid Interface Sci.* **2003**, *261*, 423–433.
36. Israelachvili, J. N. *Intermolecular and Surface Forces*, 2nd ed.; Academic Press: Suffolk, 1992.
37. Guo, Q.; Sun, X.; Palmer, R. E. Structural Dynamics Induced by Self-Assembled Monolayers on Au(111). *Phys. Rev. B* **2005**, *71*, 0354061−0354065.
38. Huang, C. M.; Wei, K. H.; Jeng, U. S.; Liang, K. S. Structural Evolution of Poly(Styrene-B-4-Vinylpyridine) Diblock Copolymer/Gold Nanoparticle Mixtures from Solution to Solid State. *Macromolecules* **2007**, *40*, 5067–5074.
39. Fernandez-Nieves, A.; Fernandez-Barbero, A.; Vincent, B.; de las Nieves, F. J. Reversible Aggregation of Soft Particles. *Langmuir* **2001**, *17*, 1841–1846.
40. Brust, M.; Walker, M.; Bethell, D.; Schiffrin, D. J.; Whyman, R. Synthesis of Thiol-Derivatized Gold Nanoparticles in a 2-Phase Liquid-Liquid System. *J. Chem. Soc., Chem. Commun.* **1994**, 801–802.